NANO LETTERS

pubs.acs.org/NanoLett

Letter

Micrometer-Scale Carrier Transport in the Solid Film of Giant CdSe/CdS Nanocrystals Imaged by Transient Absorption Microscopy

Si Li,[†] Fengrui Hu,*[,†] Yanfeng Bi, Hongyu Yang, Bihu Lv, Chunfeng Zhang, Jiayu Zhang, Min Xiao,* and Xiaoyong Wang*

Cite This: *Nano Lett.* 2023, 23, 9887−9893

Read Online

ACCESS | Metrics & More | Article Recommendations | Supporting Information

ABSTRACT: For the practical applications in solar cells and photodetectors, semiconductor colloidal nanocrystals (NCs) are assembled into a high-concentration film with carrier transport characteristics, the full understanding and effective control of which are critical for the achievement of high light-to-electricity conversion efficiencies. Here we have applied transient absorption microscopy to the solid film of giant CdSe/CdS NCs and discovered that at high pump fluences the carrier transport could reach a long distance of ∼2 μm within ∼30 ps after laser pulse excitation. This intriguing behavior is attributed to the metal−insulator transition and the associated bandlike transport, which are promoted by the enhanced electronic coupling among neighboring NCs with extended wave functions overlap of the excited-state charge carriers. Besides providing fundamental transport information in the regime of high laser pump fluences, the above findings shed light on the rational design of high-power light detecting schemes based on colloidal NCs.

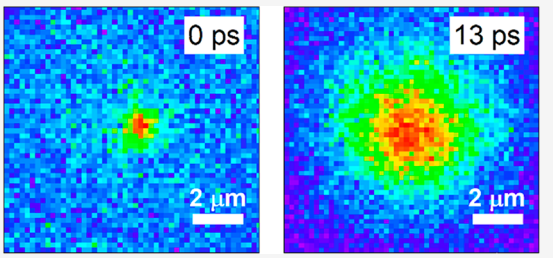

KEYWORDS: *nanocrystal, CdSe/CdS, carrier transport, metal−insulator transition, transient absorption microscopy*

Semiconductor colloidal nanocrystals (NCs) are featured with discrete energy-level structures that are tunable by the quantum-confinement effect, making them attractive building blocks for various optoelectronic devices such as lasers, light-emitting diodes, field-effect transistors, photodetectors and solar cells.[1−7] In these practical applications, high-concentration NCs are assembled into a solid film whose optoelectronic performance is critically dependent on the transport characteristics of charge carriers created by either light illumination or electrical injection. Due to the isolated nature of single NCs each containing charge carriers within a spatially confined volume, the as-formed solid film typically exhibits a short carrier transport distance of tens of nanometers and a poor carrier mobility below ∼10^{-1} cm^2 V^{-1} s^{-1}.[8−11] Over the past two decades, tremendous research efforts have been devoted to the improvement of carrier transport properties in the NCs films, mainly including the reduction of size inhomogeneity,[12−14] the change of capping ligands,[13−19] the formation of ordered arrays,[20−22] and the employment of annealing[15,16] or doping[13,23−25] procedures. So far, the longest carrier transport distance was reported to be at the scale of ∼200 nm in an ordered array of colloidal NCs.[20] Meanwhile, the highest carrier mobility of ∼20 cm^2 V^{-1} s^{-1} was obtained by annealing and sintering the solid films,[15,16] but the intrinsic electronic states of colloidal NCs would be severely perturbed or even completely destructed.

A feasible strategy of gaining high carrier mobility while keeping the quantum states intact is to induce the metal−insulator transition effect by heavy doping,[26] which requires the occupation of tens of charge carriers inside a single NC. At such a high density in conventional colloidal NCs, the charge carriers suffer from intense multiparticle Auger recombination at the picosecond time scale,[27] resulting in a much-shortened transport distance to deteriorate relevant device operations.[28,29] By adopting a thick-shell structure to reduce the overlap of electron and hole wave functions,[30,31] the Auger recombination effect can be significantly suppressed in the so-called giant CdSe/CdS NCs,[32] as confirmed by the highly efficient multiexciton emission at the single-particle level.[33] While being a suitable material to realize the long-pursued goal of electrically pumped laser diode operation,[34] these giant CdSe/CdS NCs have provided an unprecedented opportunity to explore how the transport behaviors are manifested in the presence of high-density charge carriers.

Here we focus on the solid film made of high-concentration giant CdSe/CdS core/shell NCs, whose suppressed Auger recombination yields a multiexciton lifetime longer than one nanosecond. By means of transient absorption microscopy, the carrier transport dynamics in a CdSe/CdS NCs film can be

Received: July 26, 2023
Revised: October 14, 2023
Accepted: October 17, 2023
Published: October 23, 2023

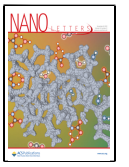

https://doi.org/10.1021/acs.nanolett.3c02788
Nano Lett. 2023, 23, 9887−9893

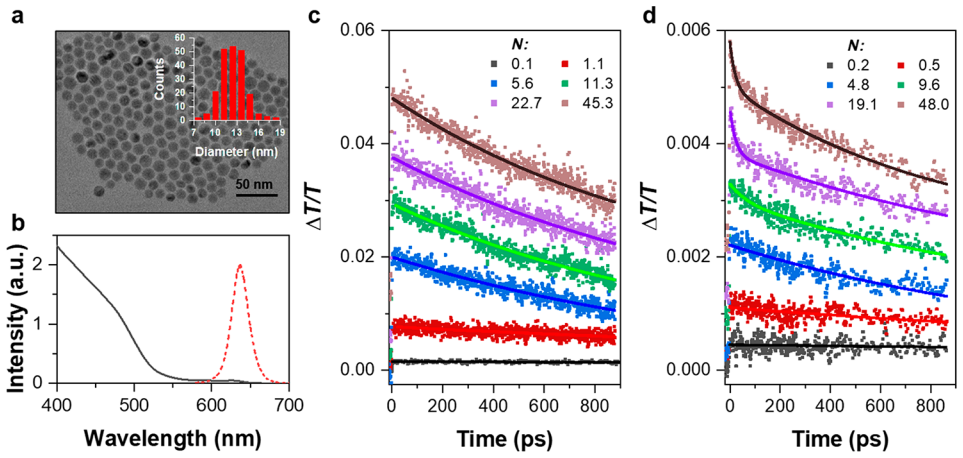

Figure 1. (a) TEM image of CdSe/CdS NCs whose statistical histogram of the diameter distribution is plotted in the inset. (b) PL (red dotted line) and absorption (black solid line) spectra of the CdSe/CdS NCs solution. (c) TA curves measured for the CdSe/CdS NCs solution at the exciton numbers (N) ranging from 0.1 to 45.3. (d) TA curves measured for the CdSe/CdS NCs film at the exciton numbers (N) ranging from 0.2 to 48. The TA curves in c and d are fitted by exponential functions with the corresponding lifetimes being listed in Table 1.

imaged with spatial and temporal resolutions of ∼100 nm and ∼200 fs, respectively. At low pump fluences, the photogenerated charge carriers are localized inside single CdSe/CdS NCs with a negligible transport distance comparable to that measured for the reference solution sample. With the increasing pump fluences, the carrier transport distance is progressively elongated and arrives at a value of ∼2 μm when ∼48 excitons are created inside a single CdSe/CdS NC. According to our Monte Carlo simulations, this long-range carrier transport is attributed to the metal−insulator transition effect triggered by the abundant charge carriers in the higher-lying energy states. The delocalized wave functions of these excited states can promote efficient electronic couplings among neighboring CdSe/CdS NCs, thus leading to the appearance of bandlike transport characteristics in the solid film.

Based on an optimized high-temperature pyrolysis method reported previously,[32,35,36] the giant CdSe/CdS core/shell NCs are synthesized with an average diameter of ∼12.4 nm (see Figure 1a). When considering the diameter of ∼3.8 nm for the CdSe core (see Figure S1), we can deduce that the shell of a single CdSe/CdS NC consists of ∼12 CdS monolayers each with a thickness of ∼0.35 nm. This chosen number of monolayers has been proved to adequately passivate the surface traps of the CdSe core and effectively avoid the strain-induced defects in the CdS shell, resulting in a photoluminescence (PL) quantum efficiency of ∼100% for the CdSe/CdS NCs.[32] As shown in Figure 1b, the band-edge absorption and emission peaks of these CdSe/CdS NCs are located at ∼625 and ∼635 nm, respectively. In Figure S2, we plot the PL intensity measured for the CdSe/CdS NCs film as a function of the laser power density, which can be fitted to yield an absorption cross section (σ) of ∼7.73×10^{-15} cm^2 at the excitation laser wavelength of 450 nm (see Supporting Information for details). This absorption cross section can be conveniently used to estimate the number of photogenerated excitons ($N = j\sigma$) inside a single CdSe/CdS NC at each pump fluence (j), which is the main parameter varied in the following transient absorption (TA) and TA microscopy (TAM) measurements performed at room temperature.

With the pump and probe wavelengths being, respectively, tuned at 450 and 635 nm, we first perform the TA measurement on a CdSe/CdS NCs solution with the toluene solvent (see the Supporting Information for details), for the purpose of probing the intrinsic carrier dynamics without the influence of mutual NC interactions. As can be seen from the TA curve measured at $N \approx 0.1$ in Figure 1c, the pump-induced transmission change of $\Delta T/T$ shows no obvious decay within $t \approx 1$ ns, which is consistent with the long single-exciton lifetime of ∼62 ns obtained from the time-resolved PL measurement (see Figure S3). With the increasing pump fluence to promote more excitons inside a single CdSe/CdS NC, there appears in the TA curve a fast decay component contributed by the multiexciton Auger recombination process.[27] Specifically, the fast decay components of ∼3.0 and ∼1.4 ns measured at $N \approx$ 1.1 and ∼5.6 should correspond to the Auger lifetimes of biexcitons and higher-order excitons, respectively. As summarized in Table 1 at various N values, this fast TA decay lifetime

Table 1. TA Decay Lifetimes of CdSe/CdS NCs Solution and Film Measured at Various Exciton Numbers (N)

CdSe/CdS NCs solution		CdSe/CdS NCs film		
N	Lifetime (ns)	N	Short lifetime (ps)	Long lifetime (ns)
1.1	2.95	0.5		2.24
5.6	1.42	4.8		1.35
11.3	1.23	9.6	68	1.40
22.7	1.34	19.1	22	1.45
45.3	1.13	48.0	21	0.86

is always longer than ∼1.1 ns even at $N > 45$, confirming that the Auger recombination of multiexcitons is indeed significantly suppressed in the giant CdSe/CdS NCs.[29,32]

After TA characterizations of the reference solution sample, we prepare a ∼80 nm-thick solid film of closely packed giant CdSe/CdS NCs (see Figure S4 for the structural properties) for the TAM measurements to probe the spatiotemporal-resolved carrier dynamics (see the Supporting Information for details). Using the TAM setup in Figure S5 with spatially overlapped pump and probe beams, we first study the carrier decay dynamics of a NCs film at different pump fluences. As shown in Figure 1d with the increasing pump fluences, there appear fast decay components with lifetimes of ∼2.2 and ∼1.4 ns at $N \approx 0.5$ and 4.8, respectively. As discussed previously for

https://doi.org/10.1021/acs.nanolett.3c02788
Nano Lett. 2023, 23, 9887−9893

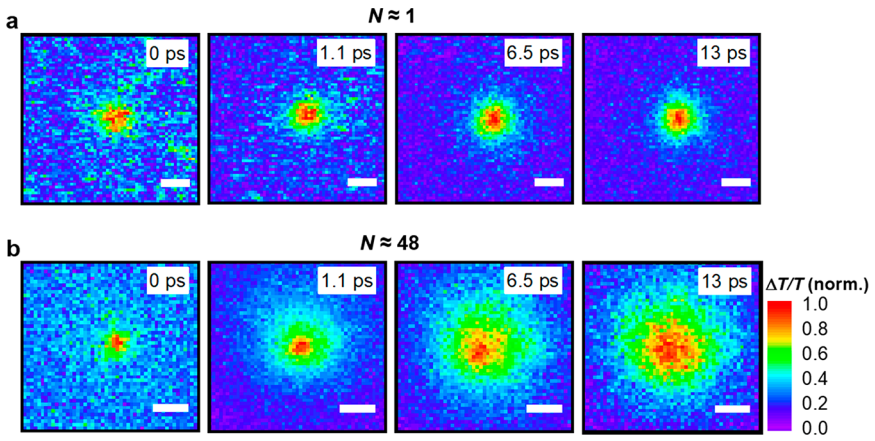

Figure 2. (a) Normalized 2D TAM images measured at $N \approx 0.1$ for the CdSe/CdS NCs film at the time delays of 0, 1.1, 6.5, and 13 ps, respectively. The scale bars represent 1 μm. (b) Normalized 2D TAM images measured at $N \approx 48$ for the CdSe/CdS NCs film at the time delays of 0, 1.1, 6.5, and 13 ps, respectively. The Scale bars represent 2 μm.

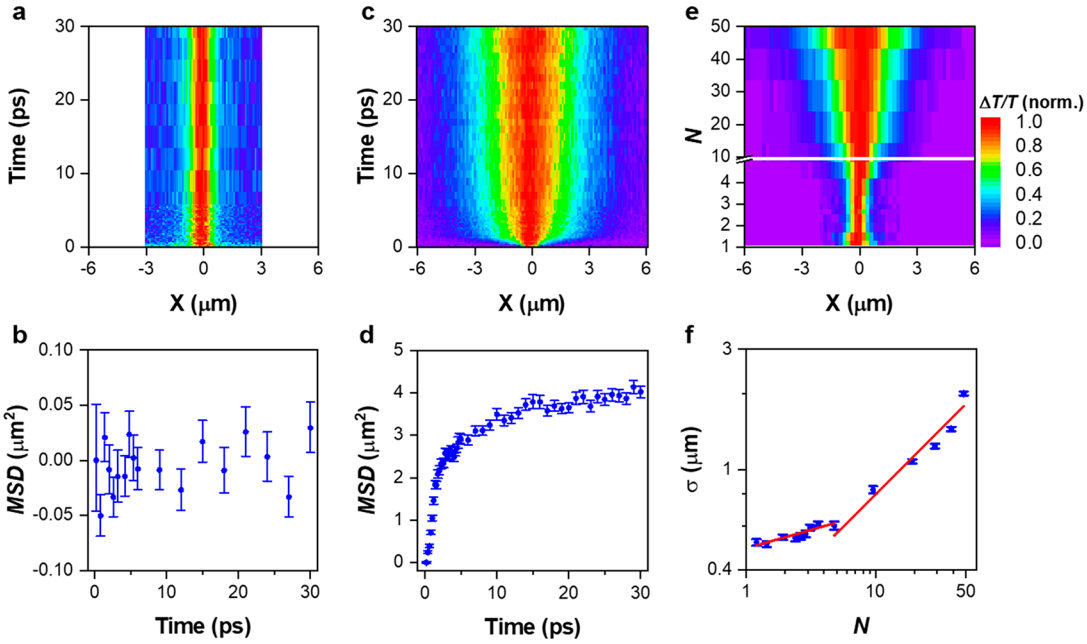

Figure 3. (a) Normalized 1D TAM image measured as a function of time delay for the CdSe/CdS NCs film excited at $N \approx 1.0$. (b) Time evolution of the corresponding MSD values extracted from a. (c) Normalized 1D TAM image measured as a function of time delay for the CdSe/CdS NCs film excited at $N \approx 48$. (d) Time evolution of the corresponding MSD values extracted from c. (e) Normalized 1D TAM image measured at a fixed time delay of 30 ps for the CdSe/CdS NCs film excited at increasing exciton numbers (N). (f) The corresponding N-dependent carrier distribution widths (σ) extracted from e where the two red solid lines are guides for the eye.

the CdSe/CdS NCs solution (Figure 1c), these two components should be contributed by the Auger recombination of biexcitons and higher-order excitons, respectively. However, as N is elevated to ~9.6 and larger numbers, besides the nanosecond component revealed above, there emerges an additional one in the TA curve with a decay lifetime of tens of picoseconds. As can be seen from the TA curves plotted in Figure 1d and the fitted values listed in Table 1, this new lifetime component becomes faster and more predominant with the increasing N.

According to previous studies,[11,20,37] the fast decay component of tens of picoseconds should be associated with the carrier transport across neighboring NCs, as further confirmed by the 2D TAM images presented below. To exclude the influence of Auger recombination with a nanosecond multiexciton lifetime (Figure 1c), these TAM measurements are performed at $t < 30$ ps. As shown in Figure 2a at the low pump fluence of $N \approx 1.0$, the spatially dependent $\Delta T/T$ distribution or carrier diffusion spot in the NCs film stays almost the same at ~0.5 μm for the variation of t from 0 to 13 ps. However, at a high pump fluence of $N \approx 48$ (Figure 2b), the carrier diffusion spot is significantly expanded to a micrometer scale during the same time period. Due to isotropic carrier diffusion in the NCs film, we can focus on 1D instead of 2D TAM images below to reduce time consumption in the optical measurement and data analysis.

The 1D TAM image taken at a low pump fluence of $N \approx 1.0$ is plotted in Figure 3a, where the $\Delta T/T$ distribution at each t up to 30 ps can be well fitted by a Gaussian function to yield the carrier distribution width $\sigma(t)$.[38,39] As plotted as a function of t in Figure 3b, the obtained mean squared displacement ($\mathrm{MSD} = \sigma^2(t) - \sigma^2(0)$) shows a small variation around the

https://doi.org/10.1021/acs.nanolett.3c02788
Nano Lett. 2023, 23, 9887−9893

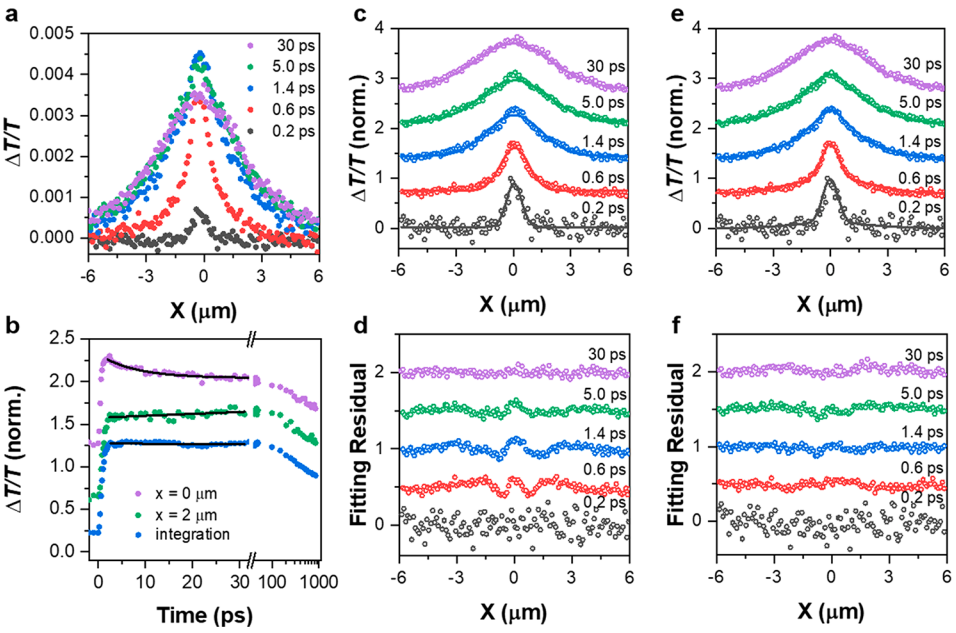

Figure 4. (a) 1D TAM profiles measured at several representative time delays for the CdSe/CdS NCs film excited at $N \approx 48$, where the raw instead of normalized data points are utilized. (b) Corresponding TA curves measured at the separation distances of $x = 0$ and 2 μm between the pump and probe laser spots, besides which the integrated one over the whole x range between ± 6 μm is also provided. (c) Normalized 1D TAM profiles of the CdSe/CdS NCs film replotted from a and fitted by the Gaussian functions. (d) Residuals of the Gaussian fittings in c. (e) Normalized 1D TAM profiles of the CdSe/CdS NCs film replotted from a and fitted by the Monte Carlo simulations. (f) Fitting residuals of the Monte Carlo simulations in e.

zero level, indicating that carrier diffusion out of the pump spot is negligible as already revealed in Figure 2a. In Figure 3c, we provide the 1D TAM image measured at a high pump fluence of $N \approx 48$, whose $\Delta T/T$ distribution now expands progressively with increasing t and arrives at a stable profile after ~28 ps. As discussed later, these $\Delta T/T$ distributions can only be roughly fitted by Gaussian functions during the fast expansion stage, with the extracted MSD values being plotted in Figure 3d to yield a long carrier transport distance ($L = \sqrt{\text{MSD}}$) of ~2.0 μm at $t > 28$ ps. In the next step, we fix the time delay at $t = 30$ ps and change the pump fluences from $N = 0-50$, with the obtained 1D TAM images being displayed in Figure 3e. As can be seen from these images and the rough Gaussian fittings of $\Delta T/T$ distributions in Figure 3f, the carrier distribution width σ starts from ~0.5 μm and increases very slightly within $N = 0-10$, after which it shows a rapid expansion to reach a large value of ~2.0 μm at $N = 50$.

For comparison, similar TAM measurements are performed on the solid films containing core-only CdSe NCs with a strong quantum confinement and giant CdSe/CdS NCs with a different types of surface ligand. In the former case, the MSD value of ~1 μm^2 extracted at 30 ps (see Figure S6) is significantly smaller than that of ~4 μm^2 measured for the giant CdSe/CdS NCs at the same pump fluence. This suggests that the enhanced Auger recombination (Figure S7) plays a crucial role in reducing the carrier transport distance in the core-only CdSe NCs film. Moreover, although there exists Förster-type energy transfer among neighboring CdSe NCs in the closely packed solid film,[21] it is not sufficient to promote long-range carrier transport observed in the giant CdSe/CdS NCs film. In the latter case, very similar MSD values are obtained after the original oleic acid ligands have been replaced by the shorter octanethiol ones (see Figure S8), thus signifying that the micrometer-scale carrier transport is robust against the variation of separation distances among neighboring giant CdSe/CdS NCs.

In Figure 4a under the $N \approx 48$ condition, we plot the raw $\Delta T/T$ profiles extracted from the 1D TAM image in Figure 3c at several representative time delays of $t = 0.2$, 0.6, 1.4, 5.0, and 30 ps, respectively. At the central position of $x = 0$ μm where the pump and probe beams are spatially overlapped, the $\Delta T/T$ signal shows a rapid rise to the maximum value within ~1.4 ps, followed by a relatively slow drop toward the end of the 30 ps time window. The above $\Delta T/T$ evolution is consistent with the TA curve measured within $t = 30$ ps at the same $x = 0$ μm position, which is plotted in Figure 4b with the purple data points. Also displayed in Figure 4b is the TA curve measured with the shifted probe beam to $x = 2$ μm, whose $\Delta T/T$ signal represented by the green data points now shows a slow rise other than the slow drop observed at $x = 0$ μm. Since the CdSe/CdS NCs located at $x = 2$ μm cannot be directly excited by the pump beam, this slow rise of the $\Delta T/T$ signal should correspond to their capture of charge carriers originally generated at $x = 0$ μm.

Besides $x = 0$ and 2 μm, we have also taken the TA measurements at many other probe-beam positions within $x = \pm 6$ μm, with the integrated curve plotted in Figure 4b by the blue data points. The $\Delta T/T$ signal remains almost a constant value within 0–30 ps, owing to the counteracting effects of charge flowing into and out of the NCs to keep the total population largely unchanged. This constant $\Delta T/T$ signal obtained within 0–30 ps also signifies that the charge population is barely influenced by the Auger recombination effect, which becomes effective only at longer time delays of $t \gtrsim 100$ ps to cause an obvious droop in the three TA curves displayed in Figure 4b.

As mentioned earlier, the $\Delta T/T$ distributions in the TAM images obtained at high pump fluences are fitted by Gaussian

https://doi.org/10.1021/acs.nanolett.3c02788
Nano Lett. 2023, 23, 9887−9893

functions only for convenience to extract the t-depenent MSD and N-dependent σ values in Figure 3d and f, respectively. In Figure 4c, we plot the normalized $\Delta T/T$ distributions originally shown in Figure 4a and fit them with the respective Gaussian functions. The fitting residuals in Figure 4d show that the $\Delta T/T$ distributions measured at 0.2 and 30 ps can be well described by the Gaussian functions, corresponding to the initial generation of charge carriers and their final arrival at equilibrium status, respectively. However, the $\Delta T/T$ distributions acquired at 0.6, 1.4, and 5.0 ps deviate significantly from the Gaussian-function fittings, giving rise to highly structured features in the fitting residuals displayed in Figure 4d. These deviations strongly imply that the diffusion of charge carriers is extremely fast with a large-step hopping behavior,[40] the essence of which can be captured by our Monte Carlo simulations (see the Supporting Information for details).

In these simulations, the carrier transport process is modeled as a combination of several random walks with the key parameters of hopping step size and time constant. To account for the long-range carrier transport, the first hopping step size and time constant are set to be ∼1.1 μm and ∼0.7 ps, respectively, which are consistent with those values previously employed to calculate the photo- and dark-band conductivities of an ordered NCs array.[25] Moreover, with the subdiffusive transport characteristics shown in Figure 3c, the hopping step size is gradually reduced with the increasing time delay in our simulations, eventually recovering the Gaussian-like carrier distribution profile after t > 28 ps. The simulated results reproduce very satisfactorily the $\Delta T/T$ distributions presented in Figure 4e, as judged by the almost unstructured fitting residuals provided in Figure 4f.

Since the micrometer-scale carrier transport occurs at the time delays of sub-30 ps, the direct excitation of NCs by means of the photon waveguiding and recycling effects can be safely ruled out, which are associated with the femtosecond and nanosecond time constants, respectively. As such, we propose that the fast carrier diffusion, featuring a large first-step hopping distance, is caused by the metal−insulator transition effect, owing to the presence of high-density charge carriers in the NCs film. According to previous theoretical calculations,[26] this metal−insulator transition is analogous to the Mott transition in bulk materials and can be triggered in a solid film when tens of excitons are accommodated by each of the composing silicon NCs. In addition, it was demonstrated in previous works that a large optical-gain bandwidth of ∼500 meV could be promoted above the band edge of giant CdSe/CdS NCs, reflecting the occupation of higher-lying energy states by the photogenerated charge carriers.[29,32] The electronic wave functions of these higher-energy charge carriers are delocalized in nature, and they are associated with a large probability density to be outside of a single NC[41,42] to facilitate the formation of extended electronic states[9,17,25] in the solid film excited at high pump fluences. This would trigger the metal−insulator transition with a bandlike carrier transport feature,[13,43] which is further confirmed by the observed quadratic dependence of MSD on the time delay[38] of ∼0−1 ps in Figure S9. When considering that the hole wave function is localized inside the core while the electron wave function is delocalized over the whole core−shell structure,[44] we speculate that the bandlike transport behavior observed in a CdSe/CdS NCs film should be caused by the photogenerated electrons with a small effective mass. Furthermore, the excited-state charge carriers are capable of participating in a hot-carrier diffusion process,[45] which could make an additional contribution to the long transport distance observed in our experiment.

In conclusion, we have performed TAM measurements on the solid film of giant CdSe/CdS core/shell NCs to characterize the carrier diffusion dynamics with high spatial and temporal resolutions. At a high pump fluence corresponding to the generation of ∼48 excitons per NC, the charge carriers demonstrate an extremely long transport distance of ∼2 μm after ∼30 ps of laser pulse excitation. A close examination of the carrier distribution spot reveals that right after the initial generation stage, it deviates significantly from the Gaussian-function fitting to imply the existence of a fast diffusion process. Based on random-walk Monte Carlo simulations, this ultrafast long-range transport is triggered by a first-step hopping size of ∼1 μm, owing to the occurrence of metal−insulator transition involving abundant charge carriers in the higher-energy excited states with extended wave functions. Once this abnormal diffusion process has started, the number of charge carriers inside each single NC gradually decreases to eventually recover their Gaussian-like spatial distributions. This subdiffusive transport behavior can also be reproduced by our Monte Carlo simulations, assuming that the hopping step size of charge carriers is gradually reduced toward the end of the ∼30 ps measurement time. The above findings have pushed electronic transport studies of colloidal NCs films to the regime of high-density charge carriers, which can stimulate the rational design of various high-power light detection and high-density charge manipulation schemes. As it is now feasible to dope a single colloidal NC with tens of extra charges by the ionic gating technique,[22] the micrometer-scale transport distance with reserved quantum features can also be employed to enhance the light-to-electricity conversion efficiencies in relevant solar-cell and photodetector devices working at normal conditions.

■ ASSOCIATED CONTENT

Supporting Information

The Supporting Information is available free of charge at https://pubs.acs.org/doi/10.1021/acs.nanolett.3c02788.

Experimental and theoretical sections; TEM image of core CdSe NCs; PL intensity measured as a function of the laser power density; PL decay curves measured at a low pump fluence; optical and structural characterizations of a NCs film; schematic diagram of the TAM optical setup; 1D TAM image and corresponding MSD of a CdSe NCs film; PL spectrum, absorption spectrum and TA decay curves of CdSe NCs; 1D TAM image and corresponding MSD of a CdSe/CdS NCs (with octanethiol ligands) film; MSD values measured at time delays from 0 to 2 ps for the CdSe/CdS and CdSe NCs films; TA decay lifetimes measured for a CdSe NC solution (PDF)

■ AUTHOR INFORMATION

Corresponding Authors

Fengrui Hu − *College of Engineering and Applied Sciences, and MOE Key Laboratory of Intelligent Optical Sensing and Manipulation, Nanjing University, Nanjing 210093, China;* orcid.org/0000-0002-8268-7373; Email: frhu@nju.edu.cn

https://doi.org/10.1021/acs.nanolett.3c02788
Nano Lett. 2023, 23, 9887−9893

Min Xiao − *National Laboratory of Solid State Microstructures, School of Physics, and Collaborative Innovation Center of Advanced Microstructures, Nanjing University, Nanjing 210093, China; Department of Physics, University of Arkansas, Fayetteville, Arkansas 72701, United States*; Email: mxiao@uark.edu

Xiaoyong Wang − *National Laboratory of Solid State Microstructures, School of Physics, and Collaborative Innovation Center of Advanced Microstructures, Nanjing University, Nanjing 210093, China*; orcid.org/0000-0003-1147-0051; Email: wxiaoyong@nju.edu.cn

Authors

Si Li − *National Laboratory of Solid State Microstructures, School of Physics, and Collaborative Innovation Center of Advanced Microstructures, Nanjing University, Nanjing 210093, China*

Yanfeng Bi − *National Laboratory of Solid State Microstructures, School of Physics, and Collaborative Innovation Center of Advanced Microstructures, Nanjing University, Nanjing 210093, China*

Hongyu Yang − *Advanced Photonic Center, Southeast University, Nanjing 210096, China*

Bihu Lv − *Department of Scientific Facilities Development and Management, Zhejiang Lab, Hangzhou 311121, China*

Chunfeng Zhang − *National Laboratory of Solid State Microstructures, School of Physics, and Collaborative Innovation Center of Advanced Microstructures, Nanjing University, Nanjing 210093, China*; orcid.org/0000-0001-9030-5606

Jiayu Zhang − *Advanced Photonic Center, Southeast University, Nanjing 210096, China*; orcid.org/0000-0001-7868-6346

Complete contact information is available at: https://pubs.acs.org/10.1021/acs.nanolett.3c02788

Author Contributions

†S.L. and F.H. contributed equally to this work

Notes

The authors declare no competing financial interest.

■ ACKNOWLEDGMENTS

This work is supported by the National Basic Research Program of China (Nos. 2021YFA1400700, 2021YFA1400803 and 2019YFA0308704), the National Natural Science Foundation of China (Nos. 62174081, 61974058, 62004092, 12274216 and 12204434), the Natural Science Foundation of Jiangsu Province (No. BK20200331), and the Priority Academic Program Development of Jiangsu Higher Education Institutions.

■ REFERENCES

(1) Kagan, C. R.; Lifshitz, E.; Sargent, E. H.; Talapin, D. V. Building Devices from Colloidal Quantum Dots. *Science* **2016**, *353*, No. aac5523.

(2) Dai, X.; Zhang, Z.; Jin, Y.; Niu, Y.; Cao, H.; Liang, X.; Chen, L.; Wang, J.; Peng, X. Solution-Processed, High-Performance Light Emitting Diodes Based on Quantum Dots. *Nature* **2014**, *515*, 96−99.

(3) Li, X.; Zhao, Y.-B.; Fan, F.; Levina, L.; Liu, M.; Quintero-Bermudez, R.; Gong, X.; Quan, L. N.; Fan, J. Z.; Yang, Z.; Hoogland, S.; Voznyy, O.; Lu, Z.-H.; Sargent, E. H. Bright Colloidal Quantum Dot Light-Emitting Diodes Enabled by Efficient Chlorination. *Nat. Photonics* **2018**, *12*, 159−164.

(4) Choi, J.-H.; Wang, H.; Oh, S. J.; Paik, T.; Sung, P.; Sung, J.; Ye, X.; Zhao, T.; Diroll, B. T.; Murray, C. B.; Kagan, C. R. Exploiting the Colloidal Nanocrystal Library to Construct Electronic Devices. *Science* **2016**, *352*, 205−208.

(5) Kozlov, O. V.; Park, Y.-S.; Roh, J.; Fedin, I.; Nakotte, T.; Klimov, V. I. Sub-Single-Exciton Lasing Using Charged Quantum Dots Coupled to a Distributed Feedback Cavity. *Science* **2019**, *365*, 672−675.

(6) Semonin, O. E.; Luther, J. M.; Choi, S.; Chen, H.-Y.; Gao, J.; Nozik, A. J.; Beard, M. C. Peak External Photocurrent Quantum Efficiency Exceeding 100% via MEG in a Quantum Dot Solar Cell. *Science* **2011**, *334*, 1530−1533.

(7) Sukhovatkin, V.; Hinds, S.; Brzozowski, L.; Sargent, E. H. Colloidal Quantum-Dot Photodetectors Exploiting Multiexciton Generation. *Science* **2009**, *324*, 1542−1544.

(8) Ginger, D. S.; Greenham, N. C. Charge Injection and Transport in Films of CdSe Nanocrystals. *J. Appl. Phys.* **2000**, *87*, 1361−1368.

(9) Yu, D.; Wang, C.; Guyot-Sionnest, P. n-Type Conducting CdSe Nanocrystal Solids. *Science* **2003**, *300*, 1277−1280.

(10) Akselrod, G. M.; Prins, F.; Poulikakos, L. V.; Lee, E. M. Y.; Weidman, M. C.; Mork, A. J.; Willard, A. P.; Bulovic, V.; Tisdale, W. A. Subdiffusive Exciton Transport in Quantum Dot Solids. *Nano Lett.* **2014**, *14*, 3556−3562.

(11) Kholmicheva, N.; Moroz, P.; Bastola, E.; Razgoniaeva, N.; Bocanegra, J.; Shaughnessy, M.; Porach, Z.; Khon, D.; Zamkov, M. Mapping the Exciton Diffusion in Semiconductor Nanocrystal Solids. *ACS Nano* **2015**, *9*, 2926−2937.

(12) Gilmore, R. H.; Lee, E. M. Y.; Weidman, M. C.; Willard, A. P.; Tisdale, W. A. Charge Carrier Hopping Dynamics in Homogeneously Broadened PbS Quantum Dot Solids. *Nano Lett.* **2017**, *17*, 893−901.

(13) Talgorn, E.; Gao, Y.; Aerts, M.; Kunneman, L. T.; Schins, J. M.; Savenije, T. J.; van Huis, M. A.; van der Zant, H. S. J.; Houtepen, A. J.; Siebbeles, L. D. A. Unity Quantum Yield of Photogenerated Charges and Band-like Transport in Quantum-Dot Solids. *Nat. Nanotechnol.* **2011**, *6*, 733−739.

(14) Lan, X.; Chen, M.; Hudson, M. H.; Kamysbayev, V.; Wang, Y.; Guyot-Sionnest, P.; Talapin, D. V. Quantum Dot Solids Showing State Resolved Band-Like Transport. *Nat. Mater.* **2020**, *19*, 323−329.

(15) Choi, J.-H.; Fafarman, A. T.; Oh, S. J.; Ko, D.-K.; Kim, D. K.; Diroll, B. T.; Muramoto, S.; Gillen, J. G.; Murray, C. B.; Kagan, C. R. Bandlike Transport in Strongly Coupled and Doped Quantum Dot Solids: A Route to High-Performance Thin-Film Electronics. *Nano Lett.* **2012**, *12*, 2631−2638.

(16) Lee, J.-S.; Kovalenko, M. V.; Huang, J.; Chung, D. S.; Talapin, D. V. Band-Like Transport, High Electron Mobility and High Photoconductivity in All-Inorganic Nanocrystal Arrays. *Nat. Nanotechnol.* **2011**, *6*, 348−352.

(17) Zhang, Z.; Sung, J.; Toolan, D. T. W.; Han, S.; Pandya, R.; Weir, M. P.; Xiao, J.; Dowland, S.; Liu, M.; Ryan, A. J.; Jones, R. A. L.; Huang, S.; Rao, A. Ultrafast Exciton Transport at Early Times in Quantum Dot Solids. *Nat. Mater.* **2022**, *21*, 533−539.

(18) Liu, Y.; Gibbs, M.; Puthussery, J.; Gaik, S.; Ihly, R.; Hillhouse, H. W.; Law, M. Dependence of Carrier Mobility on Nanocrystal Size and Ligand Length in PbSe Nanocrystal Solids. *Nano Lett.* **2010**, *10*, 1960−1969.

(19) Williams, K. J.; Tisdale, W. A.; Leschkies, K. S.; Haugstad, G.; Norris, D. J.; Aydil, E. S.; Zhu, X.-Y. Strong Electronic Coupling in Two-Dimensional Assemblies of Colloidal PbSe Quantum Dots. *ACS Nano* **2009**, *3*, 1532−1538.

(20) Penzo, E.; Loiudice, A.; Barnard, E. S.; Borys, N. J.; Jurow, M. J.; Lorenzon, M.; Rajzbaum, I.; Wong, E. K.; Liu, Y.; Schwartzberg, A. M.; Cabrini, S.; Whitelam, S.; Buonsanti, R.; Weber-Bargioni, A. Long-Range Exciton Diffusion in Two-Dimensional Assemblies of Cesium Lead Bromide Perovskite Nanocrystals. *ACS Nano* **2020**, *14*, 6999−7007.

(21) Yoon, S. J.; Guo, Z.; dos Santos Claro, P. C.; Shevchenko, E. V.; Huang, L. Direct Imaging of Long-Range Exciton Transport in Quantum Dot Superlattices by Ultrafast Microscopy. *ACS Nano* **2016**, *10*, 7208−7215.

(22) Septianto, R. D.; Miranti, R.; Kikitsu, T.; Hikima, T.; Hashizume, D.; Matsushita, N.; Iwasa, Y.; Bisri, S. Z. Enabling Metallic Behaviour in Two-dimensional Superlattice of Semiconductor Colloidal Quantum Dots. *Nat. Commun.* **2023**, *14*, 2670.
(23) Oh, S. J.; Berry, N. E.; Choi, J.-H.; Gaulding, E. A.; Paik, T.; Hong, S.-H.; Murray, C. B.; Kagan, C. R. Stoichiometric Control of Lead Chalcogenide Nanocrystal Solids to Enhance Their Electronic and Optoelectronic Device Performance. *ACS Nano* **2013**, *7*, 2413−2421.
(24) Nagpal, P.; Klimov, V. I. Role of Mid-Gap States in Charge Transport and Photoconductivity in Semiconductor Nanocrystal Films. *Nat. Commun.* **2011**, *2*, 486.
(25) Shabaev, A.; Efros, A. L.; Efros, A. L. Dark and Photo-Conductivity in Ordered Array of Nanocrystals. *Nano Lett.* **2013**, *13*, 5454−5461.
(26) Chen, T.; Reich, K. V.; Kramer, N. J.; Fu, H.; Kortshagen, U. R.; Shklovskii, B. I. Metal-Insulator Transition in Films of Doped Semiconductor Nanocrystals. *Nat. Mater.* **2016**, *15*, 299−303.
(27) Klimov, V. I.; Mikhailovsky, A. A.; McBranch, D. W.; Leatherdale, C. A.; Bawendi, M. G. Quantization of Multiparticle Auger Rates in Semiconductor Quantum Dots. *Science* **2000**, *287*, 1011−1013.
(28) Garcia de Arquer, F. P.; Talapin, D. V.; Klimov, V. I.; Arakawa, Y.; Bayer, M.; Sargent, E. H. Semiconductor Quantum Dots: Technological Progress and Future Challenges. *Science* **2021**, *373*, No. eaaz8541.
(29) García-Santamaría, F.; Chen, Y.; Vela, J.; Schaller, R. D.; Hollingsworth, J. A.; Klimov, V. I. Suppressed Auger Recombination in "Giant" Nanocrystals Boosts optical Gain Performance. *Nano Lett.* **2009**, *9*, 3482−3488.
(30) Mahler, B.; Spinicelli, P.; Buil, S.; Quelin, X.; Hermier, J.-P.; Dubertret, B. Towards Non-Blinking Colloidal Quantum Dots. *Nat. Mater.* **2008**, *7*, 659−664.
(31) Chen, Y.; Vela, J.; Htoon, H.; Casson, J. L.; Werder, D. J.; Bussian, D. A.; Klimov, V. I.; Hollingsworth, J. A. Giant" Multishell CdSe Nanocrystal Quantum Dots with Suppressed Blinking. *J. Am. Chem. Soc.* **2008**, *130*, 5026−5027.
(32) Liao, C.; Xu, R.; Xu, Y.; Zhang, C.; Xiao, M.; Zhang, L.; Lu, C.; Cui, Y.; Zhang, J. Ultralow-Threshold Single-Mode Lasing from Phase-Pure CdSe/CdS Core/Shell Quantum Dots. *J. Phys. Chem. Lett.* **2016**, *7*, 4968−4976.
(33) Htoon, H.; Malko, A. V.; Bussian, D.; Vela, J.; Chen, Y.; Hollingsworth, J. A.; Klimov, V. I. Highly Emissive Multiexcitons in Steady-State Photoluminescence of Individual "Giant" CdSe/CdS Core/Shell Nanocrystals. *Nano Lett.* **2010**, *10*, 2401−2407.
(34) Ahn, N.; Livache, C.; Pinchetti, V.; Jung, H.; Jin, H.; Hahm, D.; Park, Y.-S.; Klimov, V. I. Electrically Driven Amplified Spontaneous Emission from Colloidal Quantum Dots. *Nature* **2023**, *617*, 79−85.
(35) Carbone, L.; Nobile, C.; De Giorgi, M.; Sala, F. D.; Morello, G.; Pompa, P.; Hytch, M.; Snoeck, E.; Fiore, A.; Franchini, I. R.; Nadasan, M.; Silvestre, A. F.; Chiodo, L.; Kudera, S.; Cingolani, R.; Krahne, R.; Manna, L. Synthesis and Micrometer-Scale Assembly of Colloidal CdSe/CdS Nanorods Prepared by a Seeded Growth Approach. *Nano Lett.* **2007**, *7*, 2942−2950.
(36) Liao, C.; Fan, K.; Xu, R.; Zhang, H.; Lu, C.; Cui, Y.; Zhang, J. Laser-Annealing-Made Amplified Spontaneous Emission of "Giant" CdSe/CdS Core/Shell Nanocrystals Transferred from Bulk-Like Shell to Quantum-Confined Core. *Photonics Res.* **2015**, *3*, 200−205.
(37) Crooker, S. A.; Hollingsworth, J. A.; Tretiak, S.; Klimov, V. I. Spectrally Resolved Dynamics of Energy Transfer in Quantum-Dot Assemblies: Towards Engineered Energy Flows in Artificial Materials. *Phys. Rev. Lett.* **2002**, *89*, No. 186802.
(38) Ginsberg, N. S.; Tisdale, W. A. Spatially Resolved Photogenerated Exciton and Charge Transport in Emerging Semiconductors. *Annu. Rev. Phys. Chem.* **2020**, *71*, 1−30.
(39) Zhu, T.; Snaider, J. M.; Yuan, L.; Huang, L. Ultrafast Dynamic Microscopy of Carrier and Exciton Transport. *Annu. Rev. Phys. Chem.* **2019**, *70*, 219−244.
(40) Deng, S.; Shi, E.; Yuan, L.; Jin, L.; Dou, L.; Huang, L. Long-Range Exciton Transport and Slow Annihilation in Two-Dimensional Hybrid Perovskites. *Nat. Commun.* **2020**, *11*, 664.
(41) Tisdale, W. A.; Zhu, X.-Y. Artificial Atoms on Semiconductor Surfaces. *Proc. Natl. Acad. Sci. U. S. A.* **2011**, *108*, 965−970.
(42) Vaxenburg, R.; Rodina, A.; Lifshitz, E.; Efros, A. L. Biexciton Auger Recombination in CdSe/CdS Core/Shell Semiconductor Nanocrystals. *Nano Lett.* **2016**, *16*, 2503−2511.
(43) Kagan, C. R.; Murray, C. B. Charge Transport in Strongly Coupled Quantum Dot Solids. *Nat. Nanotechnol.* **2015**, *10*, 1013−1026.
(44) García-Santamaría, F.; Brovelli, S.; Viswanatha, R.; Hollingsworth, J. A.; Htoon, H.; Crooker, S. A.; Klimov, V. I. Breakdown of Volume Scaling in Auger Recombination in CdSe/CdS Heteronanocrystals: The Role of the Core-Shell Interface. *Nano Lett.* **2011**, *11*, 687−693.
(45) Guo, Z.; Wan, Y.; Yang, M.; Snaider, J.; Zhu, K.; Huang, L. Long-Range Hot-Carrier Transport in Hybrid Perovskites Visualized by Ultrafast Microscopy. *Science* **2017**, *356*, 59−62.

https://doi.org/10.1021/acs.nanolett.3c02788
Nano Lett. 2023, 23, 9887−9893